Functionalization of graphene oxide surfaces with phosphorus dendrimer and dendron

Omar Alami, Regis Laurent, Marine Tassé, Yannick Coppel, V. Collière, Jérôme Bignon, Jean-Pierre Majoral, Saïd El Kazzouli, Nabil El Brahmi, Anne-Marie Caminade

Functionalization of Graphene Oxide Surfaces with Phosphorus Dendrimer and Dendron

Omar Alami [a,b,c], Régis Laurent [b,c], Marine Tassé [b,c], Yannick Coppel [b,c], Vincent Collière [b,c], Jérôme Bignon [d], Jean-Pierre Majoral [b,c], Saïd El Kazzouli [a], Nabil El Brahmi [a,*], Anne-Marie Caminade [b,c,*].

[a] Euromed Research Center, Euromed Faculty of Pharmacy, Euromed University of Fes (UEMF), Route de Meknes, 30000 Fez, Morocco;
[b] Laboratoire de Chimie de Coordination du CNRS, 205 Route de Narbonne, 31077 Toulouse, CEDEX 4, France;
[c] LCC-CNRS, Université de Toulouse, CNRS, 31077 Toulouse, CEDEX 4, France
[d] Plateforme CIBI, ICSN, CNRS, Centre de Recherche de Gif, Bâtiment 27, 1 avenue de la Terrasse, 91198 Gif-sur-Yvette Cedex, France
* Correspondence: n.elbrahmi@ueuromed.org; anne-marie.caminade@lcc-toulouse.fr.

Abstract

We report a novel approach for functionalizing the graphene oxide (**GO**) surface with **AB5** phosphorus dendron, and dendrimer. First, a dendrimer was prepared having tyramine functions on the surface, while the **AB5** dendrons were synthesized and characterized having either pyridine derivatives or ethacrynic acid terminal functions and a tyramine derivative linked to the core. Subsequently, these macromolecules were grafted onto the **GO** surface *via* covalent bonding. The resulting **GO** and modified-**GO**-**AB5** dendron/dendrimer materials have been characterized by Fourier Transform Infrared (FTIR), Raman spectroscopy (RS), Thermogravimetric Analysis (TGA), Magic Angle Spinning Nuclear Magnetic Resonance (MAS-NMR) and Energy Dispersive X-ray spectroscopy (EDX) analyses. The dendritic structures and the functionalized materials were evaluated for their biological activity against HCT116 (human colon cancer), and against the non-cancerous RPE1 cells for the most active, to evaluate the safety.

Keywords: dendrons; dendrimers; graphene oxide; phosphorhydrazone;

1. Introduction

Carbon-based nanostructures, including carbon nanotubes (CNTs) and graphene, have been at the forefront of nanomaterials research over the past decade due to their unique properties and potential applications. Graphene is a two-dimensional (2D) carbon allotrope that consists of a single layer of carbon atoms arranged in a hexagonal lattice [1]. Graphene oxide (**GO**) is generally produced from graphite (superposed layers of graphene) by the "Top-Down" method [2], which uses oxidation reactions for introducing various oxygenated functional groups, followed by an exfoliation process. Graphene and **GO** possess excellent mechanical, electrical, and thermal properties, making them attractive materials for various applications [3–6]. One of the most exciting potential applications of carbon-based nanostructures is in the biomedical field [7–9]. Graphene and its oxidized form, **GO**, have gained increased attention in recent years for their potential in biomedical applications. Studies have investigated the biocompatibility and delivery ability of substances to biological targets using **GO**-based platforms [10], leading to the development of novel strategies for diagnosis and therapy. Despite the promise of carbon-based nanostructures in the biomedical field, their practical application has been hindered by several challenges. One of the main challenges is the poor solubility and biocompatibility of these materials, which limits their potential for use in biological systems [11]. To address this challenge, researchers have focused on chemical modifications to enhance their biocompatibility. One of the promising modification for carbon-based nanostructures involves the use of dendrimers and dendrons [12]. Dendrimers [13] are hyperbranched, well-defined macromolecules that are synthesized step-by-step by a repetitive process, forming a new layer with each iterative cycle. As the size and the number of terminal functions increase with the number of generations, it becomes increasingly difficult to draw the full structure. Thus, dendrimers are often represented in a linear form, with parentheses at each generation, and a number indicating the multiplication of the branches. Dendrons [14], on the other

hand, are dendritic wedges that can be considered as building blocks for the synthesis of dendrimers. The main difference between dendrons and dendrimers is the presence of a single function at the core of dendrons but not of dendrimers (Fig. 1). **AB5** phosphorus dendrons are dendritic structures issued from the cyclotriphosphazene core, in which one chloride reacted with one equivalent of reagent functionalized with a nitrogen or oxygen derivative, followed by the reaction of the five remaining chlorides with another reagent or vice versa, five chlorides reacted with five equivalents of reagent in first place followed by the reaction of the remaining chloride with another reagent [15]. Phosphorhydrazone dendrimers and **AB5** phosphorhydrazone dendrons have displayed interesting properties in various fields, including catalysis [16], fluorescence [17], biomaterials [18], and nanomedicine [19]. A particular series of phosphorhydrazone dendrimers bearing pyridine imine derivatives as terminal functions, either free or complexing diverse metals such as copper [20] or gold [21], have displayed potent anti-cancer properties. Additionally, another series of phosphorhydrazone dendrimers, which have ethacrynic acid derivative as their terminal functions [22], have shown promising results against cancer.

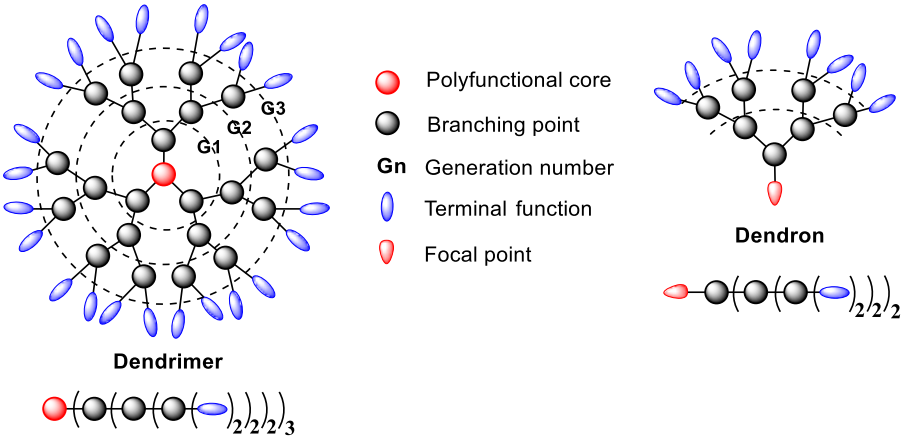

Fig. 1. Schematized structure of a dendrimer and a dendron, represented both as the full structure and in linear form with parentheses after each branching point.

To address the challenge of developing multicomponent graphene-based nanocarriers for biomedical applications, we describe a novel synthesis of a versatile graphene-based nanostructured system for oncology applications. This involves covalently conjugating phosphorus dendrimers and dendrons to the surface of **GO**. This new approach has potential for enhancing the properties of graphene oxide. Furthermore, the use of two different types of structures should afford different properties. Indeed, the presence of multiple functional groups on the surface of dendrimers may induce the reaction with several **GO** sheets, whereas the presence of a single reactive function at the core of the dendrons will induce their grafting to a single **GO** sheet.

2. Results and Discussion

*2.1. Synthesis and characterization of tyramine phosphorus dendrimer and new **AB5** phosphorus dendrons*

2.1.1. Synthesis of tyramine phosphorus dendrimer

To investigate the functionalization possibilities of **GO** surface and gain insight into the behavior of macromolecules and their reactions, we opted to synthesize a first-generation dendrimer with tyramine on its surface. The presence of the tyramine moiety allows for the formation of a covalent bond through an amidation reaction between the dendrimer's amine functions and carboxylic acid functions of **GO**. The commonly used method for the synthesis of the desired dendrimer is a divergent approach that involves repeating two key steps starting from a cyclotriphosphazene core (as previously reported [23]). The first step involves nucleophilic substitution of the chlorine atoms by 4-hydroxybenzaldehyde, resulting in the formation of a dendrimer with six surface aldehyde functions, referred to as **G'0**. The dendrimer is then grown through a condensation reaction between the aldehydes of **G'0** and dichlorothiophosphorhydrazide **2**, which is obtained by reacting methylhydrazine with $P(S)Cl_3$ at -60

°C. The advancement of the condensation reaction is monitored by the vanishing of the aldehyde group signal in the ^{1}H NMR spectra. Dendrimer **3-G$_1$** was obtained with a high yield of 88%. To synthesize phenol **4**, the amine group of tyramine was protected using Boc_2O. The functionalized phenol **4** was then reacted with **3-G$_1$** to produce **4-G$_1$** as we reported before [24] in a satisfactory yield of 89%. The deprotection of the Boc-protected amines was achieved using trifluoroacetic acid (TFA). This was accomplished by adding a mixture of TFA and DCM (dichloromethane) to a solution of dendrimer **4-G$_1$.** The reaction was monitored by using ^{1}H NMR until the Boc functional group peak disappears completely. The resulting deprotected dendrimer **4a-G$_1$** was obtained with a yield of 98% (Scheme 1).

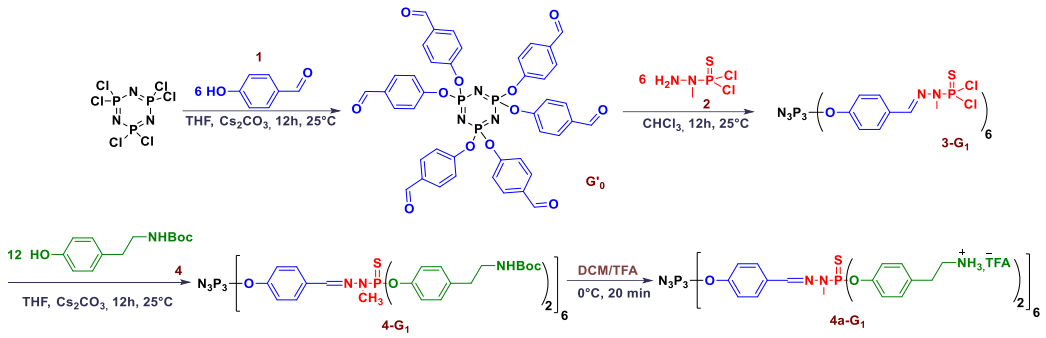

Scheme 1. Synthesis of the first generation dendrimer **4a-G$_1$**.

*2.1.2. Synthesis of new **AB5** phosphorus dendrons*

Our goal in synthesizing new ***AB5*** phosphorus dendrons is to create an asymmetric structure that contains a distinct functional group, to form a single covalent bond with the **GO** surface. Instead of utilizing hexachlorocyclotriphosphazene ($N_3P_3Cl_6$) with six surface benzaldehydes, commonly used in classical dendrimers, we have devised a penta-substituted asymmetric core, **AB5**, incorporating five 4-hydroxybenzaldehyde groups and a single chloride. In the first step, five equivalents of 4-hydroxybenzaldehyde were grafted to $N_3P_3Cl_6$, affording the pentaaldehyde **5** [14]. The second step concerned the functionalization of the pentaaldehyde **5** with phenol **4**. Compound **5-G$_0$** was isolated in 88% yield. The growing of the dendron was then carried out by condensation reaction between the aldehydes and the dichlorothiophosphorhydrazide **2**. The condensation reaction was monitored by the disappearance of the signal of the aldehyde groups in ^{1}H NMR. Dendron **5-G$_1$** was isolated in 81% yield (Scheme 2). The ^{31}P{^{1}H} NMR spectrum of product **5-G$_1$** exhibits two distinct areas of signals. The first peak, originating from the core, appears at 8.3 ppm. The second area of signals presented three peaks for the **$PSCl_2$** groups centered at 62.5 ppm with a relative intensity of 2:1:2. This phenomenon can be attributed to the geometry of the cyclotriphosphazene core, which is depicted as a planar structure with three branches above and three below the cycle. Consequently, one phosphorus atom of the dendron experiences a different chemical environment than the others, resulting in the observed NMR signals. A similar observation has been reported for another dendron [25].

The synthesis of dendrons is feasible up to the second or third generation. However, we opted to stop the growth at the first generation to retain the accessibility of the function attached to the core. This decision was based on our earlier findings, where we established that only the first generation dendrons possessing thioctic acid at the core, could be successfully grafted onto a gold surface. The second generation dendrons, in which the core was less accessible, were found unsuitable for this purpose, as previously reported [26].

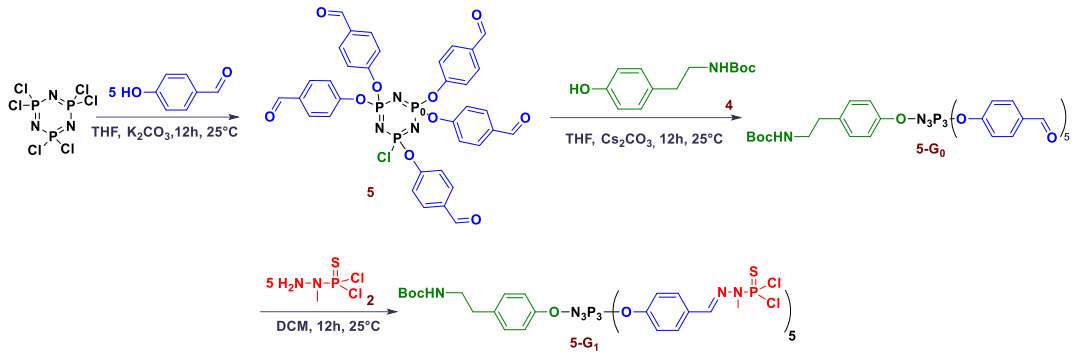

Scheme 2. Synthesis of the first generation of **AB5** dendron **5-G1**.

The next step in the synthesis of the **AB5** dendrons involved surface decoration with various phenol-pyridine derivatives and ethacrynic acid (**EA**) derivative. The synthesis of these compounds was achieved through previously reported works [22,27,28]. Compound **6a** was prepared by reacting tyramine with 2-pyridine carboxaldehyde, while **6b** was obtained through the condensation of tyramine with di(2-pyridyl) ketone [27]. Compound **6c** was synthesized by condensing 4-hydroxybenzaldehyde with 2-hydrazinopyridine [28], and compound **6d** was obtained by amidation of **EA** and 4-(piperazin-1-yl)phenol [22]. Next, compounds **6a-d** were reacted with the first-generation dendron **5-G1** under basic conditions to obtain dendrons **6a-d-G1** (Scheme 3) in the yield range between 45-78%. Every dendron underwent characterization through the use of ^{31}P NMR spectroscopy. The results showed two singlets for the P(S)(OAr)$_2$ groups in all compounds, with a ratio of 2:3 (Fig. 2).

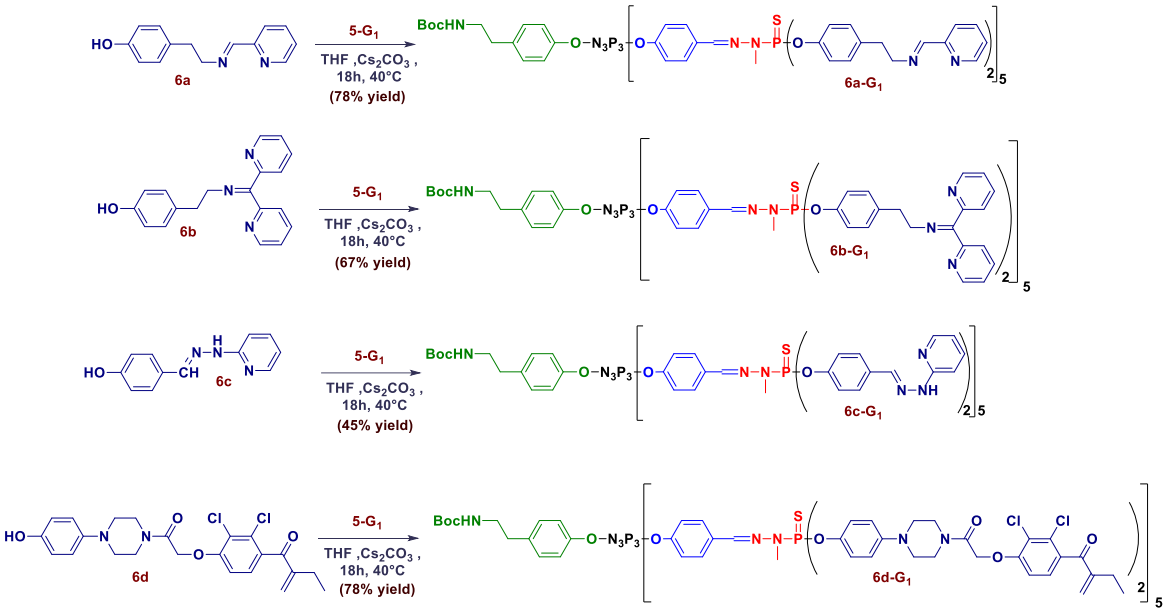

Scheme 3. Functionalization of **5-G1** with phenol-pyridine derivatives **6a-c** and **EA** derivative **6d**.

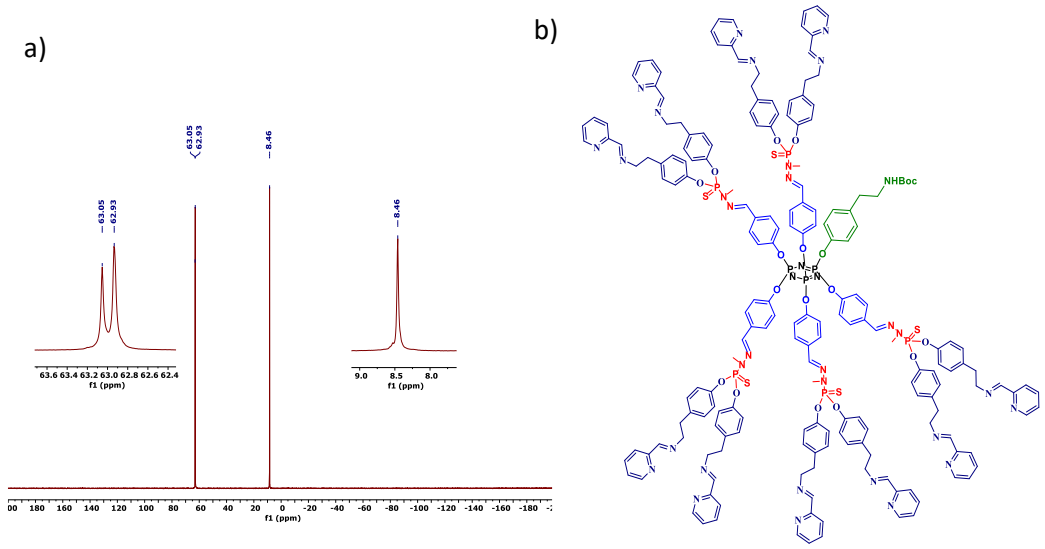

Fig. 2. (**a**) $^{31}P\{^{1}H\}$ NMR spectrum of dendron **6a-G1**, with the 2 signals in the left insert corresponding to the P=S groups in a 2:3 ratio; (**b**) Full chemical structure of **6a-G1** showing 2 P=S groups up and 3 P=S groups down, relative to the cyclotriphosphazene ring.

The deprotection of the **6a-d-G1** dendrons was attempted in a similar approach to that of the **4a-G1** dendrimer, as descripted before (Scheme 4). However, for the **6a-G1** and **6c-G1** dendrons, the reaction monitored by $^{31}P\{^{1}H\}$ NMR displayed multiple signals, which were unexpected as normally only two signals would be detected for the P=S groups. These various signals may arise due to protonation of the dendrons, degradation, hydrolysis or transformation of P=S into P=O. Indeed, the decomposition of the dendrimers **6a-G1** and **6c-G1,** which have the same internal structure and differ only in the nature of the surface groups, under the conditions of deprotection of the Boc group is due to the presence of easily accessible imine functions in **6a** and **6c**, which are not stable in the acid medium, where they undergo protonation and subsequent decomposition. Moreover, the asymmetrical nature of the dendrons makes characterization a more challenging task. In contrast, the $^{31}P\{^{1}H\}$ NMR of **6b-G1** and **6d-G1** dendrons indicate that the dendritic structure was preserved, unlike to the previous deprotection examples. The ^{1}H NMR spectrum confirms the total deprotection of Boc-protected tyramine as shown by the disappearance of the Boc signal at 1.36 ppm for **6d-G1**, which was isolated with a yield of 95%. However, in the case of **6b-G1**, we encountered limitations in achieving full Boc deprotection and we decided to not grafting this dendron onto the surface of **GO** (Scheme 4).

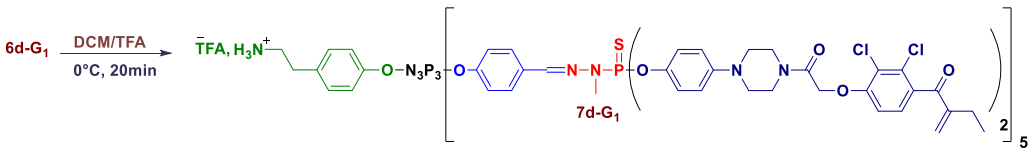

Scheme 4. Deprotection of dendron **6d-G1**

*2.2. Synthesis and characterization of modified **GO***

Graphene oxide (**GO**) was produced from graphite through the Hummers method [29], which involves a stepwise addition of H_2SO_4, $NaNO_3$, and $KMnO_4$ to the graphite. This process results in the formation of graphite oxide, which can subsequently be exfoliated into individual **GO** nanosheets using sonication techniques in organic solvents like *N*,*N*-dimethylformamide (DMF) and tetrahydrofuran (THF) [11], ultimately yielding the desired **GO**. The chemical structure of **GO** is complex and contains a variety of functional groups. The ^{13}C MAS NMR spectrum of our **GO** reveals several distinctive peaks, including an epoxy function (C-O-C) at 61 ppm, a peak at around 70 ppm attributed to hydroxyl functions (C-OH), and another at 133 ppm corresponding to sp2 carbon atoms. Other signals are also observed at 101, 167, and 191 ppm, which are attributed to the lactol (O-C-O), carboxylic acid (O-C=O),

and ketone (C=O) functional groups, respectively. Attesting to the characterization of this material, the IR spectra reveal the presence of the carboxylic acid vibration at 1723 cm^{-1} (C=O) and the vibration at 1619 cm^{-1} corresponding to the C=C bond. The Raman spectroscopy technique can be used to characterize **GO** by displaying bands corresponding to non-polar but polarizable bonds, including C=C bonds. In the prepared **GO**, three main signals were observed in the Raman spectra, which are the 1340 cm^{-1} signal D (defect), 1580 cm^{-1} signal G (C=C), and 2700 cm^{-1} signal 2D (corresponding to layer stacking). The intensity of signal D can be modified when introducing defects, such as structural defects or hybridization modification from sp2 to sp3, which happens when substituents are grafted onto the **GO** structure. I_D/I_G ratio is sensitive to the sp2 hybridization of carbon atoms and can be influenced by factors such as the introduction of defects. Therefore, changes in the I_D/I_G ratio can provide information about the structural modification of **GO**. Thermogravimetric analysis (TGA) is a valuable tool for evaluating the thermal stability of carbon derivatives. When applied to our **GO**, the resulting TGA curve demonstrates that **GO** is inherently unstable when exposed to heat, leading to a two-step decomposition process as described in the literature [30].

To utilize **GO** in the amidation reaction, it was essential to modify some of its functional groups, specifically by activating the acidic groups. This was accomplished by transforming carboxylic acid to carbonyl chloride *via* the use of $SOCl_2$, resulting in the formation of **GO-COCl** (Scheme 5). While this material was not characterized due to its high susceptibility to hydrolysis, it was directly utilized in the reaction with a dendron and a dendrimer.

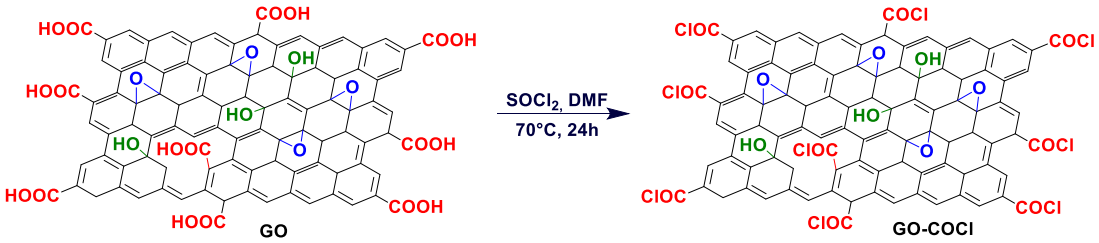

Scheme 5. Illustration of the synthesis of **GO** modified with $SOCl_2$

*2.3. Grafting dendrimer and dendron to modified **GO***

Having in hand the modified graphene oxide **GO-COCl**, the subsequent step involved the grafting of suitably functionalized dendrimer and dendron. To achieve this, the modified graphene oxide **GO-COCl** was dispersed in DMF using sonication for 20 minutes, then a mixture of dendrimer **4a-G_1** or dendron **7d-G_1**, along with triethylamine (NEt_3) in DMF, was added. The resulting mixture was left at room temperature (25°C) for 72 hours, resulting in the production of functionalized materials **4a-G_1@GO** (Scheme 6A) and **7d-G_1@GO** (Scheme 6B). During the process, the resulting black powder was precipitated in ether, followed by centrifugation and several washings with MeOH to remove the excess of dendrimer or **AB5** dendron. Subsequently, the black solids of **4a-G_1@GO** and **7d-G_1@GO** were dried under vacuum. It is important to note that the functionalization of the **GO** surface is a complex chemical process and is never complete. The reaction takes place randomly, and it is not limited to only two -COOH groups. The scheme 6 illustrates the reaction between dendron/dendrimer and **GO** for clarity. Various techniques were employed to verify the presence of dendrimer and dendron linked to **GO**.

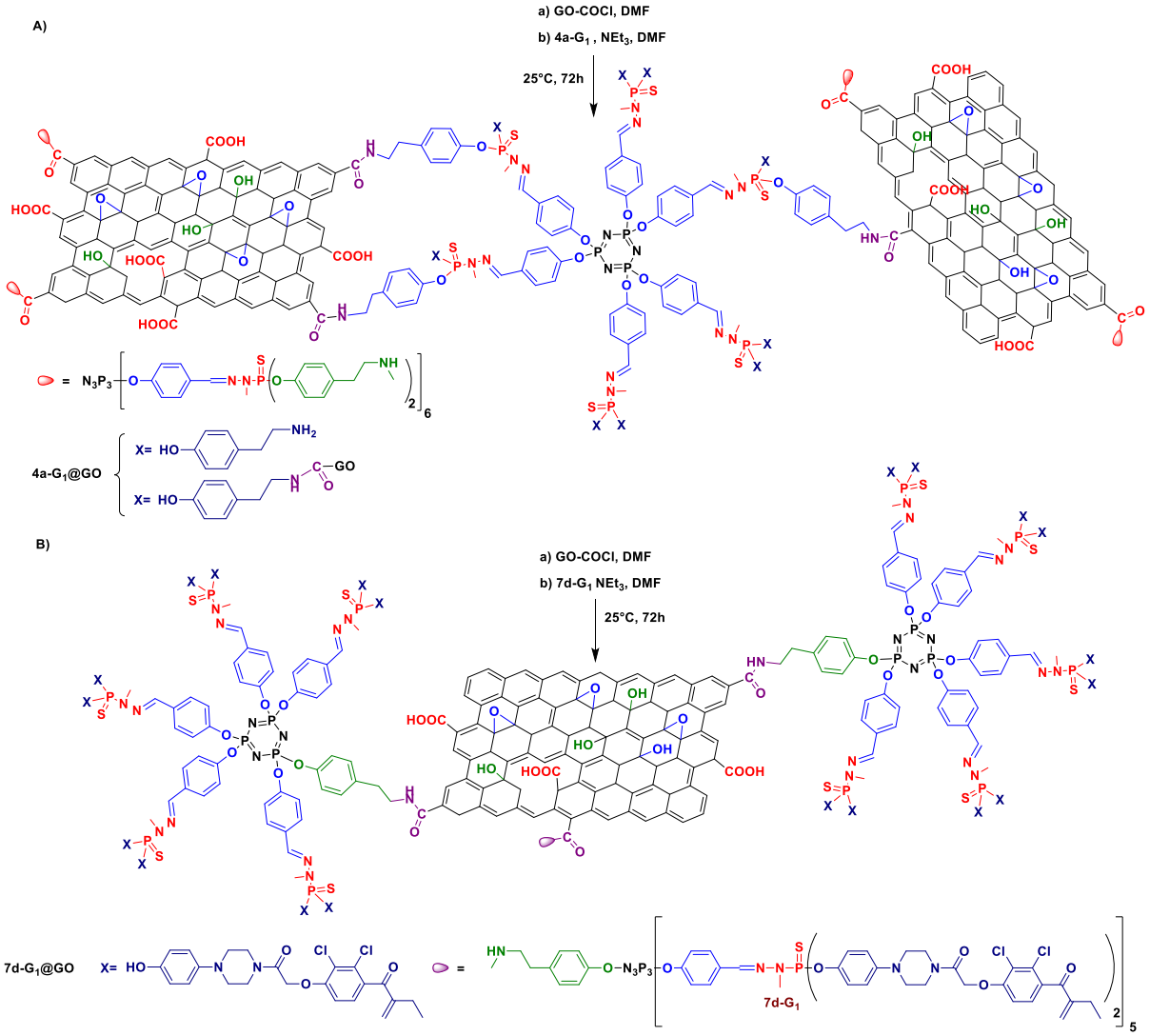

Scheme 6. Amidation reaction between **4a-G1** dendrimer, and **7d-G1** dendron with **GO-COCl**, affording the materials **4a-G1@GO** (A) and **7d-G1@GO** (B), respectively. These drawings are only an illustration of one of the possible structures of the materials.

^{31}P MAS NMR revealed the existence of two signals at approximately 8 and 64 ppm, corresponding to the N_3P_3 core and P(S)(OAr)$_2$ terminal functions, respectively, as exemplified for **4a-G1@GO** (Fig. 3a). Raman spectroscopy provides valuable insights into the grafting of dendrimer and dendron, with a significant modification of the I_D/I_G ratios. The I_D/I_G ratios obtained for **4a-G1@GO** and **7d-G1@GO** hybrid materials are 1.11 and 1.09, respectively. The I_D/I_G ratios obtained for the hybrid materials are higher than the observed I_D/I_G ratio for unmodified **GO**, which is 0.8, indicating a significant modification to the **GO** structure resulting from the grafting of dendrimer and dendron (Fig. 3b).

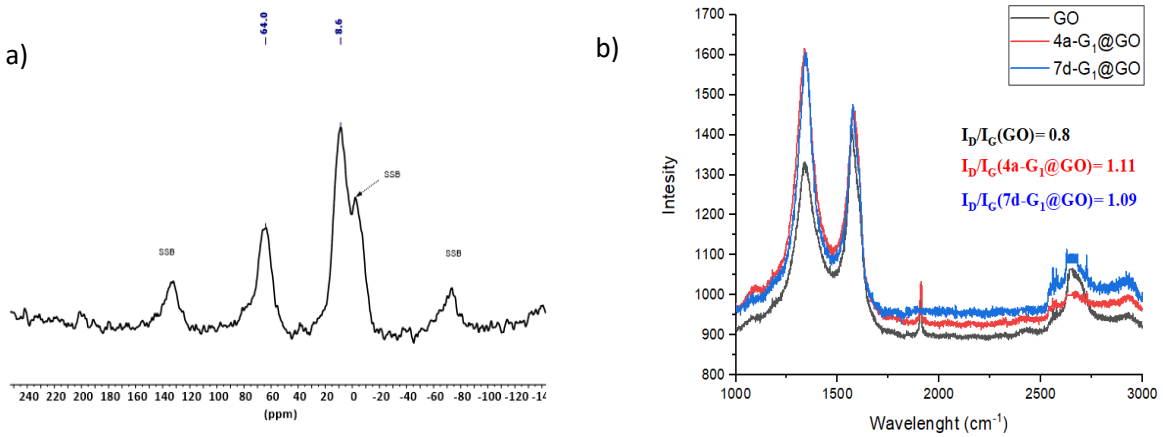

Fig. 3. Characterization of material **4a-G1@GO.** (**a**) ^{31}P MAS NMR of **4a-G1@GO**; (**b**) Raman spectra of **GO** (black), **4a-G1@GO** (red) and **7d-G1@GO** (blue).

The infrared spectra (IR) clearly confirm the successful grafting of both the dendron and dendrimer onto **GO**, as demonstrated by a comparative analysis of the IR spectra for **GO**, dendrimer **4a-G1**, and **4a-G1@GO** (Figure 4a). Specifically, the IR spectrum of the material functionalized with the dendrimer **4a-G1@GO** clearly exhibits the characteristic peaks of the carboxylic acid functions of the **GO** (C=O) at 1723 cm^{-1}, as well as the unique fingerprint of the dendrimer **4a-G1**. This observation can be attributed to the steric hindrance provided by the dendrimer, which prevents full accessibility to all the modified carboxylic acid functions on the surface of the **GO**.

Fig. 4b shows the combined TGA results of **GO,** dendrimer **4a-G1**, and material **4a-G1@GO** under air. **GO** undergoes a two-step decomposition process. In the first stage, which occurs at around 100°C, the material loses 20% of its weight due to the removal of water molecules and residual solvents embedded within the **GO** structure. The second stage occurs around 200°C, resulting in a substantial loss of mass (~ 30%) due to the decomposition of oxygenated functional groups. Dendrimer **4a-G1** undergoes a three-step decomposition process, with weight losses of approximately 5%, 25%, and 50% in the first, second, and third stages, respectively. In the first stage of decomposition, occurring at around 200°C, the material loses approximately 5% of its weight due to the removal of water molecules and residual solvents from within the dendrimer structure. The second stage, taking place around 380°C, leads to a mass loss of approximately 25% and corresponds to the decomposition of oxygenated functional groups. The third stage, occurring at 430°C, results in a mass loss of approximately 50% due to the decomposition of the dendrimer skeleton. Material **4a-G1@GO** undergoes three distinct stages during thermal analysis. The first stage, occurring around 250°C, shows a 5% weight loss due to the removal of residual solvents present in the **GO** structure. The second stage, around 380°C, corresponds to the decomposition of tyramine and some surface functions of **GO**. Finally, at approximately 520°C, a 55% weight loss is observed due to the decomposition of both **GO** functions and the dendrimer skeleton. Interestingly, the presence of the dendrimer on the surface of **GO** provides greater thermal stabilization.

The same interpretation is applied for the dendron, **7d-G1** and material **7d-G1@GO** as well (see SI).

To confirm the functionalization of **GO** surface with different dendron and dendrimer, elementary analysis was realized, based on the content in sulfur. Indeed, sulfur is only a component of the dendrimer and dendron used in this study, thus the content in sulfur of the materials will indicate the quantity of dendritic structures grafted. The results shown in Table 1 indicate the presence of sulfur in all grafted materials **4aG1@GO** and **7d-G1@GO**, but in different proportions. The lower percentage of grafting is observed with the dendrimer (**4a-G1**). Indeed, the presence of 12 amine functions on the surface of this dendrimer induces the possibility to interact with several functions on a **GO** sheet, and even to interact with two **GO** sheets, thus preventing the access to other molecules. On the contrary, the dendron **7d-G1** has a single function at the core for interacting with **GO**, and thus a larger quantity can be grafted. Anyway, these data do confirm that the phosphorus dendrimer and dendron have effectively bonded to **GO**, creating new composite materials.

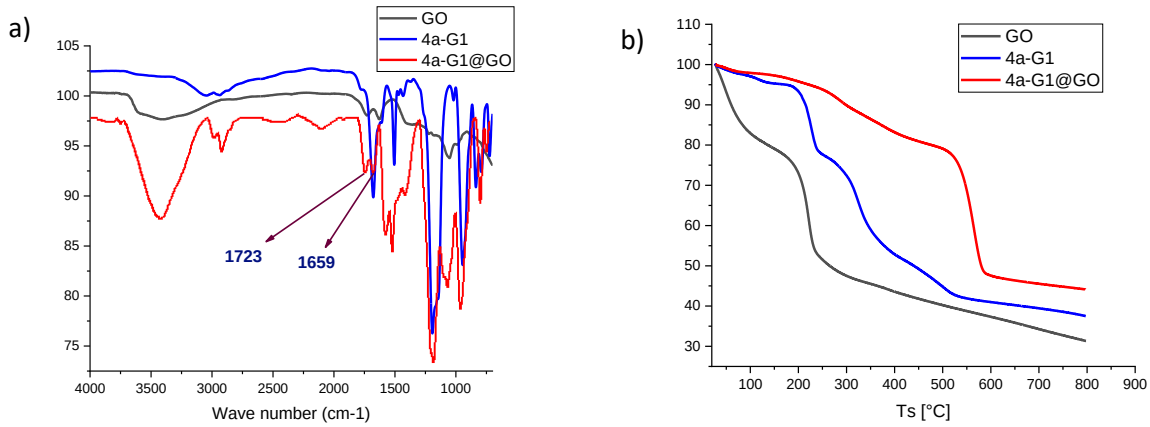

Fig. 4. Characterization of material **4a-G1@GO,** (**a**) IR spectra of **GO** (black), dendrimer **4a-G1** (blue), and **4a-G1@GO** (red); (**b**) TGA curves of **GO** (black), dendrimer **4a-G1** (blue), and **4a-G1@GO** (red), under air.

Table 1

Elemental analysis of sulfur for the obtained materials **4a-G1@GO** and **7d-G1@GO.**

Material	theoretical S%	measured S%	% of compound grafted (dendrimer or dendron)	Mol. of compound/g of material
4a-G1@GO	3.47	0.65	19	$5.77\ 10^{-5}$
7d-G1@GO	1.32	1.14	86	$7.62\ 10^{-5}$

In order to further characterize the materials, Energy Dispersive X-ray spectroscopy (EDX) analyses were performed. Fig. 5 presents Scanning Electron Microscopy (SEM) images alongside the EDX spectra of **GO** and **4a-G1@GO**. The EDX investigation of **GO** reveals the presence of carbon and oxygen, accompanied by a minor percentage of sulfur (0.1 %), stemming from residual remnants of oxidation process by H_2SO_4. The EDX mapping of **4a-G1@GO** demonstrated in addition the presence of phosphorus (0.3%) and the presence of sulfur with an increase of 0.2%, warrants the presence of **4a-G1**. The presence of a small quantity of chlorine is due to **COCl** residual of **GO-COCl.** The absence of nitrogen in the analysis of **4a-G1@GO** is due to the non-fully quantitative analysis provided by the technique, in particular for light elements such as nitrogen or phosphorus, especially when present in low quantities. In addition, in the EDX spectrum of **7d-G1@GO** (Supplementary Information), a distinctive profile emerges, portraying the coexistence of phosphorus (0%), sulfur (0.3%) and, nitrogen (4.1%), together with chlorine (3.7%), which is due to the ethacrynic acid on the surface of **7d-G1**. The presence of these elements serves as a compelling indicator of the presence of **7d-G1** onto the surface of **GO**.

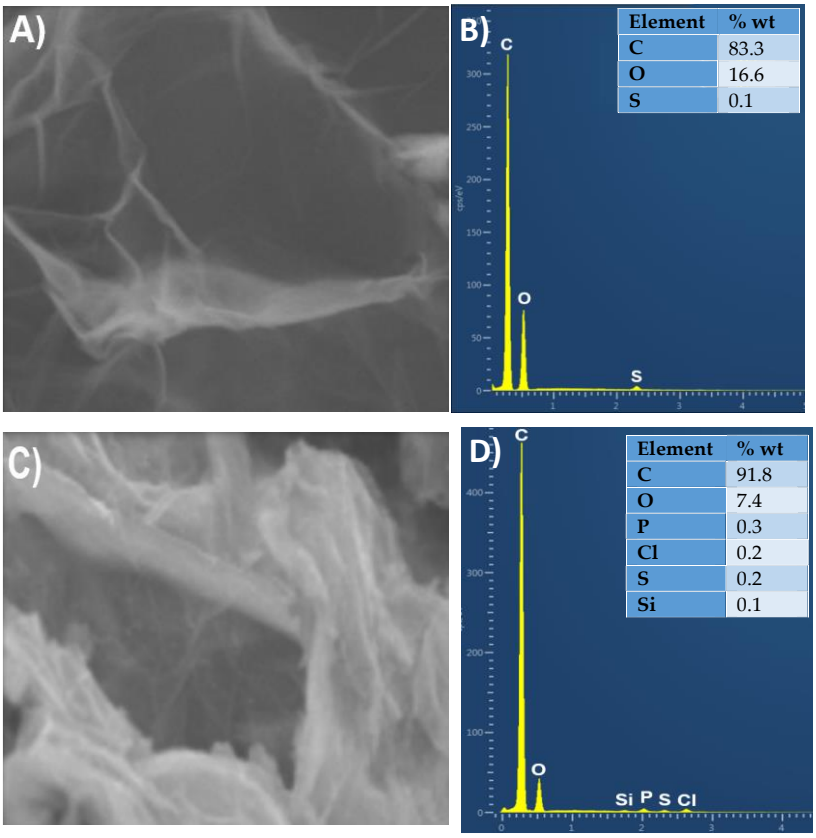

Fig. 5. Characterization of materials **GO** and **4a-G1@GO,** (**a**) SEM image of **GO** (**b**) EDX data of **GO** (c) SEM image of **4a-G1@GO** (d) EDX data of **4a-G1@GO**.

*2.4. Biological tests of dendrons, dendrimer, and **GO** functionalized with macromolecules.*

Recently, our team has demonstrated the effectiveness of dendrimers with derivatives of pyridine as terminal groups, both free and bound to metals, against various cancer cell lines *in vitro*. The most potent compounds were third-generation dendrimers with pyridine imine terminal groups [20,28]. Additionally, other studies have utilized dendrimers with **EA** against cancer cells [22]. Thus, it was crucial to investigate the recently synthesized materials. We evaluated several of the compounds synthesized, using the cancerous cell line HCT116 (human colon cancer). It is worth noting that all compounds were soluble in stock solutions (10^{-2} M in DMSO), but precipitated in the medium and on cells. We also evaluated the most active compounds towards non-cancerous RPE1 cells (Human retinal pigment epithelial-1), a non-transformed alternative to cancer cell lines. Experiments were conducted in triplicate for 72 hours at two concentrations (10^{-5} and 10^{-6} M) in DMSO, except for **4a-G1** in DMF. The results in Table 1 indicate that the hydrazine pyridine dendron (**6c-G1**) and the dendrimer (**4a-G1)** are active at 10^{-5} M (but not at 10^{-6} M), while the pyridine imine and **EA** dendrons (**6d-G1** and **6a-G1**) are not active against HCT116. These results are contradictory with our previous experiments [22,28], but the 3-dimensional structure of third generation dendrimers and first generation dendrons are obviously very different, and some of us have shown the tremendous importance of the 3-D structure of dendrimers on their biological properties [31]. To verify the safety of the active compounds, the next step involved testing them against the non-cancerous RPE1 cells, under the same conditions as with the HCT116 cell line. However, it was found that the dendrimer and the dendrons were as toxic to the non-cancerous cells as they were to the cancerous cells (Table 2).

Table 2

Anti-proliferative activities of dendrons in DMSO towards the cancerous cell line HCT116, and the non-cancerous cells RPE1.

Dendrons and	**HCT116 cells[a]**	**RPE1 cells[a]**

dendrimer				
	% viability at 10^{-5} M[b]	% viability at 10^{-6} M[b]	% viability at 10^{-5} M[b]	% viability at 10^{-6} M[b]
4a-G1 [c,d,e]	27.2 (±1.6)	97.6 (±2.9)	1.3 (±1.3)	100.4 (±2.0)
6a-G1 [c,d]	98.8 (±0.7)	98.1 (±1.2)	-	-
6c-G1 [c,d]	17.7 (±4.4)	91.3 (±3.3)	9.4 (±1.4)	101.2 (±1.7)
6d-G1 [c,d]	75.9 (±4.0)	97.9 (±0.5)	-	-

[a] measures made in triplicate, [b] dendron or dendrimer concentration, [c] precipitated in medium, [d] precipitated on cells, [e] solubilized in DMF

Two types of materials were then tested: **GO** alone and **GO** functionalized. Both were tested under the same conditions. The tests were performed using stock dispersions of the materials at a concentration of 10^{-3} M in DMSO, but the materials precipitated in the medium and on cells. The results showed that **GO** alone had weak toxicity towards cancerous HCT116 cells at a concentration of 10^{-5} M (Table 3). The grafting of dendron and dendrimer to **GO** did not provide any improvement, thus the materials were not tested on non-cancerous cells.

Table 3

Anti-proliferative activities of **GO** and **GO** functionalized with dendrimer or dendron in DMSO towards the cancerous cell line HCT116.

Dendron or dendrimer grafted to GO	HCT116 cells[a]	
	% viability at 10^{-5} M[b]	% viability at 10^{-6} M[b]
GO	80.0 (±3.5)	102.1 (±3.4)
4a-G$_1$@GO [c,d]	93.1 (±2.1)	97.5 (±0.8)
7d-G$_1$@GO [c,d]	89.9 (±1.7)	96.0 (±3.0)

[a] measures made in triplicate, [b] dendron or dendrimer concentration, [c] precipitated in medium. [d] precipitated on cells.

3. Materials and Methods

3.1. General information

All reactions were carried out under an inert atmosphere using standard Schlenk techniques, and manipulations were conducted using a vacuum line. Commercially available chemicals were used as received from Sigma Aldrich, Acros, Fluka, and Alfa Aesar. Dry tetrahydrofuran (THF) was obtained from the MBraun MB-SPS-800 solvent drying system under an argon atmosphere. Unless otherwise specified, all other solvents were used as supplied commercially. Analytical thin-layer chromatography (TLC) was performed on aluminum plates coated with silica gel 60 F254. If necessary, reaction mixtures were purified by column chromatography on silica gel (230-400 mesh) using a gradient solvent system as the eluent. ^{1}H, ^{13}C, and ^{31}P NMR spectra were recorded at 298 K using Bruker AV 300 and Bruker AV 400 spectrometers. Coupling constants are reported in Hz and chemical shifts are reported in ppm relative to tetramethylsilane (TMS) for ^{1}H NMR and ^{13}C-{^{1}H} NMR. ^{31}P chemical shifts were referenced to an external 85% H_3PO_4 sample. First-order signals are indicated as follows: s (singlet), d (doublet), t (triplet), q (quadruplet). ^{13}C NMR signals were assigned using JMOD, HMQC, and HMBC sequences as necessary. The numbering used for the attribution of NMR signals is shown in Fig. 6. MAS NMR spectra were obtained using a Bruker AvanceIII HD 400WB instrument at 298K with several spinning rates (SR) to differentiate isotopic peaks from spinning sidebands. Raman spectra were recorded at 298K using a full-power 532 nm laser, with 20-second acquisition and 4 accumulations between 1000 and 3000 cm^{-1}. Infrared (IR) vibrational spectroscopy was performed at 298 K on a Perkin Elmer 100 FT-IR spectrometer, using a germanium crystal. Thermogravimetric analysis (TGA) was carried out under air atmosphere using a Mettler TGA DSC 3+ instrument. Elementary analysis was carried out using Perkin Elmer 2400 Series II Flash Combustion Analyzer. Scanning electron microscopy (SEM) images and energy dispersive X-ray (EDX) analysis were taken on a high-end field emission scanning electron

microscope (FEG) equipped with an EDS SDD spectrometer (JSM-7800F Prime). Transmission electron microscopy (TEM) images and energy dispersive X-ray (EDX) analysis were taken on a field-corrected emission transmission electron microscope probes and is coupled to an EDX spectrometer and an energy loss spectrometer (EELS). (JEM-ARM200F Cold FEG). Both analyses were carried out at the "Centre de Microcaractérisation Raimond Castaing", Toulouse, France.

The synthesis of compound **4** was accomplished following the methodology outlined in reference [31], while the preparation of dendrimers **4-G1** and **4a-G1** was performed as described in reference [24], compound **5** was synthesized following the procedure mentioned in reference [32]. The synthesis of monomers **6a** and **6b** was conducted in accordance with the protocol detailed in reference [27], while the preparation of compounds **6c** and **6d** was carried out in accordance with the protocol detailed in references [28] and [22], respectively.

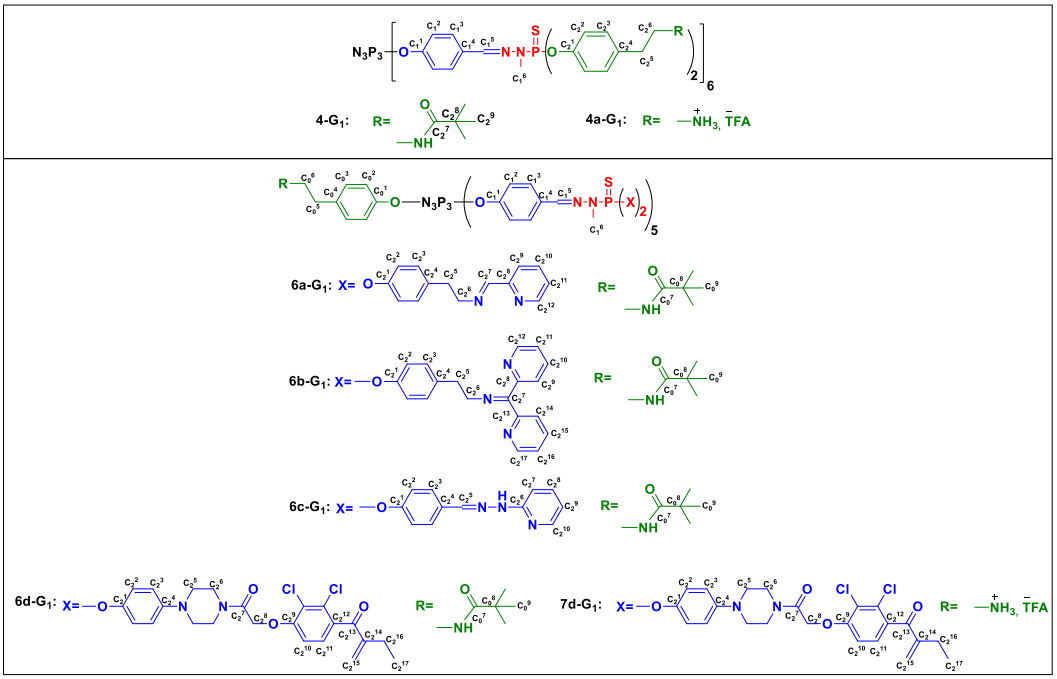

Fig. 6. Numbering for NMR signals assignment.

*3.2 General 3-step synthesis strategy for the **6a-d-G1** familly of dendrons*

a) To a solution of pentaaldehyde **5** (2.06 mmol, 1.6 g) and cesium carbonate (4.12 mmol, 1.35 g) in THF (7 ml), a solution of Boc-tyramine **4** (2.47 mmol, 0.59 g) in THF (7 ml) was added. The reaction mixture was stirred at room temperature overnight. The salts were removed by centrifugation and the clear solution was concentrated under reduced pressure. The residue was then dissolved in the minimum amount of THF (4 ml) and precipitated in 100 ml of pentane/ether (4/1). Product **5-G0** was recovered as a colorless oil which became a white powder after one night under reduced pressure, isolated in 88% yield.

b) To a solution of **5-G0** (1.23 mmol, 1.2 g) in DCM (5 mL) was added a solution of $H_2NNMePSCl_2$ **2** in $CHCl_3$ (8.60 mmol, 33.6 mL). The reaction mixture was stirred overnight at room temperature. The solvent was removed under reduced pressure. The residue was then dissolved in the minimum amount of $CHCl_3$ (4 mL) and precipitated in 100 mL of pentane/ether (4/1). The resulting powder was filtered and the procedure was repeated twice. Dendron **5-G1** was obtained with a yield of 81% as a white powder.

c) To a solution of **5-G1** (0.28 mmol, 0.5 g) and cesium carbonate (5.91 mmol, 1.92 g) in THF (5 mL) was added a solution of phenol **6a** (2.95 mmol, 0.67 g), **6b** (2.95 mmol, 0.90 g), **6c** (2.96 mmol, 0.63 g), or **6d** (from **5-G1,** 0.11 mmol, 0.2 g; cesium carbonate, 2.48 mmol, 0.82 g; and **6d,** 1.18 mmol, 0.55 g) in THF (7 mL). The reaction mixture was stirred at room temperature for one night. The salts were removed by centrifugation and the clear solution was concentrated under reduced pressure. The residue was then dissolved in the minimal amount of THF (4 mL) and precipitated in 100 mL of pentane/ether (1/1), with

the exception of **6b-G1**, for which the precipitate was washed with MeOH at 0°C. The resulting powder was filtered and the procedure repeated twice (precipitated with pentane at the end) to give the desired product as a white powder in 78% yield for **6a-G1**, 45% yield for **6b-G1**, 67% yield for **6c-G1** and 78% yield for **6d-G1**.

3.3 General strategy for deprotection of dendrimer and dendrons

To prepare **4a-G1**, compound **4-G1** (310 mg, 0.073 mmol) was dissolved in a mixture of DCM/TFA (2 ml/2 ml) at 0°C for 20 minutes. After evaporating the residual solvent, the crude product was washed with 10 ml of MeOH and dried under vacuum to remove excess TFA by co-evaporation. This process was repeated three times, resulting in a 98% yield of **4a-G1** as a yellowish powder. Similarly, dendrons **6b-G1** (30 mg, 0.0067 mmol) and **6d-G1** (30 mg, 0.0049 mmol) were each dissolved in a mixture of DCM/TFA (1 ml/1 ml) at 0°C for 20 minutes. The residual solvent was then evaporated under vacuum, and the crude product obtained from each was washed with 5 ml of MeOH and dried under vacuum to remove excess TFA by co-evaporation. This procedure was repeated three times for each compound. Compound **7b-G1** could not be fully purified, but compound **7d-G1** was isolated with a yield of 95% as a yellow powder. The purity of the products was confirmed by phosphorus NMR and proton NMR. The attribution of NMR signals is made according to Figure 6.

6a-G1. $^{31}P\{^1H\}$ NMR (121 MHz, $CDCl_3$) δ 63.05 (s, P=S), 62.93 (s, P=S), 8.46 (s, P=N). ^1H NMR (300 MHz, $CDCl_3$) δ 8.61 (d, *J* = 4.9 Hz, 10H, $\boldsymbol{C_2^{12}}$), 8.26 (s, 10H, $\boldsymbol{C_2^7}$), 7.92 (d, *J* = 7.9, 10H, $\boldsymbol{C_2^9}$), 7.70– 7.52 (m, 25H, $\boldsymbol{C_1^3, C_1^5, C_2^{10}}$), 7.31 – 7.25 (m, 10H, $\boldsymbol{C_2^{11}}$), 7.16 – 6.91 (m, 54H, $\boldsymbol{C_0^2, C_0^3, C_1^2, C_2^2, C_2^3}$), 4.70 (br s, 1H, NH), 3.85 (q, *J* = 7.2 Hz, 20H, $\boldsymbol{C_2^6}$), 3.24 (m, 17H, $\boldsymbol{C_1^6}$, $\boldsymbol{C_0^6}$), 2.96 (q, *J* = 7.2 Hz, 20H, $\boldsymbol{C_2^5}$), 2.67 (t, *J* = 7.4 Hz, 2H, $\boldsymbol{C_0^5}$), 1.38 (s, 9H, $\boldsymbol{C_0^9}$). $^{13}C\{^1H\}$ NMR (75 MHz, $CDCl_3$) δ 162.38 (s, $\boldsymbol{C_2^7}$), 155.8 (s, $\boldsymbol{C_0^7}$), 154.34 (s, $\boldsymbol{C_2^8}$) 151.25 (m, $\boldsymbol{C_0^1}$, $\boldsymbol{C_1^1}$), 149.45 (s, $\boldsymbol{C_2^{12}}$), 148.98 (d, *J* = 7.2 Hz, $\boldsymbol{C_2^1}$), 138.48 (d, *J* = 14.01 Hz, $\boldsymbol{C_1^5}$), 136.90 (s, $\boldsymbol{C_2^4}$), 136.54 (s, $\boldsymbol{C_2^{10}}$), 136.05 (s, $\boldsymbol{C_1^4}$), 132.11 (s, $\boldsymbol{C_0^4}$), 129.98 (s, $\boldsymbol{C_2^3}$), 129.81 (s, $\boldsymbol{C_0^3}$), 128.22 (s, $\boldsymbol{C_1^3}$), 124.73 (s, $\boldsymbol{C_2^{11}}$), 121.30 (s, $\boldsymbol{C_1^2}$), 121.26 (s, $\boldsymbol{C_0^2}$), 121.23 ($\boldsymbol{C_2^2}$), , 120.99 (s, $\boldsymbol{C_2^9}$), 77.24 (s, $\boldsymbol{C_0^8}$), 62.67 (s, $\boldsymbol{C_2^6}$), 41.71 (s, $\boldsymbol{C_0^6}$), 36.59 (s, $\boldsymbol{C_2^5}$), 35.45 (s, $\boldsymbol{C_0^5}$), 33.01 (m, $\boldsymbol{C_1^6}$), 28.41 (s, $\boldsymbol{C_0^9}$).

6b-G1. $^{31}P\{^1H\}$ NMR (121 MHz, $CDCl_3$) δ 63.09 (s, P=S), 62.99 (s, P=S), 8.43 (s, P=N). ^1H NMR (300 MHz, $CDCl_3$) δ 8.66 (m, 10H, $\boldsymbol{C_2^{12}}$), 8.48 (m, 10H, $\boldsymbol{C_2^{17}}$), 8.06 (m, 10H, $\boldsymbol{C_2^{14}}$), 7.75 – 7.49 (m, 35H, $\boldsymbol{C_1^3, C_1^5, C_2^{10}, C_2^{15}}$), 7.21 (m, 20H, $\boldsymbol{C_2^{11}, C_2^{16}}$), 7.10 – 6.90 (m, 64H, $\boldsymbol{C_0^2, C_0^3, C_1^2, C_2^2, C_2^3, C_2^9}$), 4.74 (s, 1H, NH), 3.65 (m, 19H, $\boldsymbol{C_2^6}$), 3.22 (m, 17H, $\boldsymbol{C_1^6, C_0^6}$), 2.99 (m, 20H, $\boldsymbol{C_2^5}$), 2.67 – 2.59 (m, 2H, $\boldsymbol{C_0^5}$), 1.38 (s, 9H, $\boldsymbol{C_0^9}$). $^{13}C\{^1H\}$ NMR (75 MHz, $CDCl_3$) δ 167.05 (s, $\boldsymbol{C_2^7}$), 156.69 (s, $\boldsymbol{C_2^{13}}$), 155.81 (s, $\boldsymbol{C_0^7}$), 155.17 (s, $\boldsymbol{C_2^8}$), 151.24 (s, $\boldsymbol{C_0^1, C_1^1}$), 149.57 (s, $\boldsymbol{C_2^{12}}$), 149.20 (s, $\boldsymbol{C_2^1}$), 148.85 (s, $\boldsymbol{C_2^{17}}$), 138.61 (s, $\boldsymbol{C_1^5}$), 137.44 (s, $\boldsymbol{C_2^4}$), 136.79 (s, $\boldsymbol{C_0^4}$), 136.39 (s, $\boldsymbol{C_2^{15}}$), 136.10 (s, $\boldsymbol{C_2^{10}}$), 132.19 (s, $\boldsymbol{C_1^4}$), 130.03 (s, $\boldsymbol{C_2^3}$), 129.82 (s, $\boldsymbol{C_0^3}$), 128.23 (s, $\boldsymbol{C_1^3}$), 124.18 (s, $\boldsymbol{C_2^{16}}$), 123.54 (s, $\boldsymbol{C_2^9}$), 123.12 (s, $\boldsymbol{C_2^{11}}$), 122.30 (s, $\boldsymbol{C_2^{14}}$), 121.15 (m, $\boldsymbol{C_0^2}$, $\boldsymbol{C_1^2}$, $\boldsymbol{C_2^2}$), 79.06 (s, $\boldsymbol{C_0^8}$), 55.28 (s, $\boldsymbol{C_2^6}$), 41.72 (s, $\boldsymbol{C_0^6}$), 36.63 (s, $\boldsymbol{C_2^5}$), 35.45 (s, $\boldsymbol{C_0^5}$), 32.95 (m, $\boldsymbol{C_1^6}$), 28.44 (s, $\boldsymbol{C_0^9}$).

6c-G1. $^{31}P\{^1H\}$ NMR (121 MHz, THF) δ 63.06 (s, P=S), 62.94 (s, P=S), 8.57 (s, P=N). ^1H NMR (300 MHz, THF) δ 9.95 (s, 10H, NH).8.06 (dd, *J* = 5.0, 1.8 Hz, 10H, $\boldsymbol{C_2^{10}}$), 7.85 – 7.81 (m, 10H, $\boldsymbol{C_2^5}$), 7.80 – 7.68 (m, 15H, $\boldsymbol{C_1^3, C_1^5}$), 7.63 (m, 20H, $\boldsymbol{C_2^3}$)7.56 – 7.48 (m, 10H, $\boldsymbol{C_2^8}$), 7.32 – 7.21 (m, 30H, $\boldsymbol{C_2^7, C_2^2}$), 7.19 – 7.06 (m, 10H, $\boldsymbol{C_1^2}$), 7.04 (d, *J* = 8.2 Hz, 2H, $\boldsymbol{C_0^3}$), 6.93 (d, *J* = 8.2 Hz, 2H, $\boldsymbol{C_0^2}$) 6.72 – 6.62 (m, 10H, $\boldsymbol{C_2^9}$), 6.04 (s, 1H, NHBoc), 3.44 – 3.28 (m, 15H, $\boldsymbol{C_1^6}$), 3.20 (t, *J* = 7.2 Hz, 2H, $\boldsymbol{C_0^6}$), 2.69 (t, *J* = 7.2 Hz, 2H, $\boldsymbol{C_0^5}$), 1.40 (s, 9H, $\boldsymbol{C_0^9}$). $^{13}C\{^1H\}$ NMR (75 MHz, THF) δ 157.40 (s, $\boldsymbol{C_2^6}$), 155.69 (s, $\boldsymbol{C_0^7}$), 151.46 (br s, $\boldsymbol{C_0^1, C_1^1}$,), 150.76 (m, $\boldsymbol{C_2^1}$), 147.66 (s, $\boldsymbol{C_2^{10}}$), 139.24 (m, $\boldsymbol{C_1^5}$), 137.21 (s, $\boldsymbol{C_2^5}$, $\boldsymbol{C_2^8}$), 133.25 (s, $\boldsymbol{C_2^4}$), 132.45 (s, $\boldsymbol{C_1^4}$), 132.37 (s, $\boldsymbol{C_0^4}$), 129.63 (s, $\boldsymbol{C_0^3}$), 128.14 (s, $\boldsymbol{C_1^3}$), 127.04 (s, $\boldsymbol{C_2^3}$), 121.48 (d, *J* = 4.4 Hz, $\boldsymbol{C_2^2}$), 121.16 (s, $\boldsymbol{C_1^2}$), 120.70 (s, $\boldsymbol{C_0^2}$), 114.79 (s, $\boldsymbol{C_2^9}$), 106.49 (s, $\boldsymbol{C_2^7}$), 77.56 (s, $\boldsymbol{C_0^8}$), 32.51 (m, $\boldsymbol{C_1^6}$), 27.80 (s, $\boldsymbol{C_0^6}$), 24.73 (s, $\boldsymbol{C_0^5}$), 24.45 (s,$\boldsymbol{C_0^9}$).

6d-G1. $^{31}P\{^1H\}$ NMR (121 MHz, CD_2Cl_2) δ 64.86 (s, P=S), 64.82 (s, P=S), 9.27 (s, P=N). ^1H NMR (300 MHz, CD_2Cl_2) δ 7.69 – 7.56 (m, 15H, $\boldsymbol{C_1^3, C_1^5}$), 7.16 – 6.91 (m, 52H, $\boldsymbol{C_1^2, C_2^2, C_2^{10}, C_2^{11}}$), 6.86 – 6.72 (m, 22H, $\boldsymbol{C_0^2, C_2^3}$), 5.93 (s, 10H, $\boldsymbol{C_2^{15}}$), 5.57 (s, 10H, $\boldsymbol{C_2^{15}}$), 4.84 (m, 20H, $\boldsymbol{C_2^8}$), 4.70 (s, 1H, NH), 3.67 (m, 40H, $\boldsymbol{C_2^6}$), 3.31 – 3.15 (m, 17H, $\boldsymbol{C_0^6, C_1^6}$), 3.08 (m, 40H, $\boldsymbol{C_2^5}$), 2.65 (t, *J* = 7.4 Hz, 2H, $\boldsymbol{C_0^5}$), 2.47 – 2.38 (m, 20H, $\boldsymbol{C_2^{16}}$), 1.36 (s, 9H, $\boldsymbol{C_0^9}$), 1.12 (t, *J* = 7.4 Hz, 30H, $\boldsymbol{C_2^{17}}$). $^{13}C\{^1H\}$ NMR (75 MHz, CD_2Cl_2) δ 196.92 (s, $\boldsymbol{C_2^{13}}$), 165.22 (s, $\boldsymbol{C_2^7}$), 155.97 (s, $\boldsymbol{C_0^7}$), 155.82 (s, $\boldsymbol{C_2^{11\prime}}$), 151.59 (br s, $\boldsymbol{C_0^1, C_1^1}$), 150.55 (s, $\boldsymbol{C_2^{14}}$), 149.00 (s, $\boldsymbol{C_2^4}$), 144.42 (s, $\boldsymbol{C_2^1}$), 138.89 (m, $\boldsymbol{C_1^5}$), 133.92 (s, $\boldsymbol{C_2^{10\prime}}$), 132.77 (m, $\boldsymbol{C_0^4, C_1^4}$), 131.41 (s, $\boldsymbol{C_2^9}$), 130.26 (s, $\boldsymbol{C_0^3}$), 129.00 (s, $\boldsymbol{C_2^{15}}$), 128.59 (s, $\boldsymbol{C_1^3}$), 127.48 (s, $\boldsymbol{C_2^{11}}$), 122.92

(s, C_2^{12}), 122.26 (s, C_2^2), 121.69 (s, C_1^2), 121.19 (s, C_0^2), 117.73 (s, C_2^3), 111.28 (s, C_2^{10}), 79.03 (s, C_0^8), 68.65 (s, C_2^8), 51.16 (s, C_0^6), 50.27 (s, $C_2^{5\prime}$), 49.71 (s, C_2^5), 45.48 (s, $C_2^{6\prime}$), 42.25 (s, C_2^6), 35.79 (s, C_0^5), 33.43 (m, C_1^6), 28.51 (s, C_0^9), 23.80 (s C_2^{16}), 12.85 (s, C_2^{17}).

7d-G1. $^{31}P\{^1H\}$ NMR (121 MHz, CD_2Cl_2) δ 62.10 (s, P=S), 61.8 (s, P=S) 7.79 (s, P=N). ^1H NMR (300 MHz, CD_2Cl_2) δ 7.72 – 7.62 (m, 15H, C_1^5, C_1^3), 7.54 – 7.49 (m, 20H, C_2^3), 7.39 – 7.36 (m, 20H, C_2^2), 7.19 – 7.09 (m, 22H, C_0^3, C_1^2, C_2^{11}), 6.95 – 6.86 (m, 12H, C_0^2, C_2^{10}), 6.00 (s, 10H, C_2^{15}), 5.60 (s, 10H, C_2^{15}), 4.93 (s, 20H, C_2^8), 4.12 (s, 40H, C_2^6), 3.66 (s, 40H, C_2^5), 3.37 – 3.32 (m, 15H, C_1^6), 3.13 (s, 2H, C_0^6), 2.84 (s, 2H, C_0^5), 2.42 (q, *J* = 7.4 Hz, 20H, C_2^{16}), 1.11 (t, *J* = 7.4 Hz, 30H, C_2^{17}).

*3.4 Strategy for the synthesis of **GO***

Graphitic oxide was prepared by stirring 10 g of graphite and 5 g of sodium nitrate in 230 ml of sulfuric acid. The reagents were mixed in a 2-liter three-neck flask which had been cooled to 0°C in an ice bath. Maintaining vigorous stirring, 30 g of potassium permanganate was added to the suspension. The speed of addition was carefully controlled to prevent the suspension temperature from exceeding 20°C. The ice bath was then removed, and the temperature of the suspension increased to 35°C for 30 minutes. After 30 minutes, 460 ml of water was slowly added, causing an exothermic reaction and a temperature rise to 98°C. The suspension was maintained at this temperature for 15 minutes. Then, 1 liter of lukewarm water was added, followed by treatment with 37% hydrogen peroxide until gassing stopped. The suspension was filtered and washed three times with water. The dry form of graphite oxide was obtained by centrifugation (10,000 rpm, 40 min) followed by drying in a freeze dryer for 48 hours, resulting in a brown powder.

*3.5 General strategy for grafting dendrimer and dendron onto **GO***

The synthesis of new materials was carried out in two steps: a) **GO** (50 mg) was treated with thionyl chloride (35 ml) in the presence of 0.5 ml of DMF in a 50 ml Schlenk flask at 70°C under argon for 24 h. The excess of $SOCl_2$ was removed under reduced pressure, the functionalized graphene oxide was washed with THF, and filtered on a PVDF filter membrane. The procedure was repeated three times and the product **GO-COCl** was obtained as a black powder (too unstable to be characterized). b) To a solution of **GO-COCl** (50 mg) and synthesized dendrimer **4a-G1**, or dendron **7d-G1** (50 mg) in 20 ml of DMF in a 100 ml Schlenk flask, triethylamine (2 ml) was added under an argon atmosphere, followed by sonication for 30 minutes. The reaction mixture was stirred at room temperature for 72 h. Then, the resulting mixture was poured into 300 ml of diethyl ether to precipitate the product. The black precipitate was recovered by centrifugation at 10,000 rpm for 25 min. The resulting black powder was washed with MeOH, followed by sonication and another centrifugation. The procedure was repeated twice, and the material was dried with a freeze dryer. The dendrimer and dendron immobilized on **GO**, **4a-G1@GO** and **7d-G1@GO** were recovered as a black powder.

4a-G1@GO: ^{31}P MAS NMR (162 MHz, SR=14 kHz) δ 64.0 (P=S), 8.6 (P=N). IR υ= 3400 (OH), 1723 (C=O), 1659 (N-C=O) cm^{-1}. RAMAN D (1340), G (1580) cm^{-1}. Anal. Calcd: S, 3.47. Found: S, 0.65.

7d-G1@GO: ^{31}P MAS NMR (162 MHz, SR=14 kHz) δ 62.3 (P=S), 7.3 (P=N). IR υ= 3400 (OH), 1658 (C=O, N-C=O) cm^{-1}. RAMAN D (1340), G (1580) cm^{-1}. Anal. Calcd: S, 1.32. Found: S, 1.14.

Biological tests. Cell lines were obtained from the American type Culture Collection (ATCC, Rockville, MD) and were cultured according to the supplier's instructions. Briefly, human HCT-116 colorectal carcinoma cells were grown in Gibco McCoy's 5A supplemented with 10% fetal calf serum and 1% glutamine. Human hTERT-RPE1 cells were cultured in DMEM/F12 medium containing 10% fetal calf serum and 1% glutamine. Cell lines were maintained at 37°C in a humidified atmosphere containing 5% CO_2. Cell viability was determined by a luminescent assay according to the manufacturer's instructions (Promega, Madison, WI, USA). Briefly, the cells were seeded in 96-well plates (2.5×10^3 cells/well) containing 90 μL of growth medium. After 24 h of culture, the cells were treated with the tested compounds at 1 and 10 μM final concentrations. Control cells were treated with the vehicle. After 72 h of incubation, 100 μL of CellTiter Glo Reagent was added for 15 min before

recording luminescence with a spectrophotometric plate reader PolarStar Omega (BMG LabTech). The percent viability index was calculated from three experiments.

4. Conclusion and outlook

To sum up, we have described a new approach for grafting **AB5** phosphorus dendron and dendrimer onto **GO**, using the tyramine motif as the end-group on the dendrimer or the core in the case of **AB5** dendron having **EA** derivatives as terminal functions, on the surface of **GO**. The resulting hybrid materials were characterized by employing FTIR, Raman spectroscopy, TGA, and MAS NMR analyses. Elemental analyses of sulfur confirmed the grafting of dendrimer and dendron, with a higher efficiency for the dendron than for the dendrimer. SEM-EDX analyses confirmed the grafting of the dendrimer and dendron. Some of the dendritic compounds display a moderate anti-cancer activity towards the HCT116 cell line, but this activity was almost entirely lost in the hybrid nanocomposites, probably due to the poor solubility of the **GO**-functionalized materials in biological media, even at low concentration.

CRediT authorship contribution statement

Conceptualization, N.E.B. and A.M.C.; methodology, N.E.B., S.E.K. and A.M.C.; validation, O.A., M.T., Y.C., J.P.M., and J.B.; investigation, O.A., M.T., Y.C., V.C. and J.B.; resources, N.E.B and A.M.C.; data curation, R.L.; writing—original draft preparation, O.A. and N.E.B.; writing—review and editing, N.E.B., S.E.K., R.L. J.P.M. and A.M.C.; visualization, O.A.; supervision, N.E.B. and A.M.C.; project administration, N.E.B. and A.M.C.; funding acquisition, N.E.B. and A.M.C. All authors have read and agreed to the published version of the manuscript.

Funding

This research was funded by TOUBKAL/19/88, grant number 41405WE,

Declaration of Competing Interest

The authors declare that they have no known competing financial interests or personal relationships that could have appeared to influence the work reported in this paper.

Data availability

Data will be made available on request.

Acknowledgments

Authors acknowledge PHC-TOUBKAL, CAMPUS FRANCE, LCC and UEMF (Scholarships in Morocco) for funding. The Paul Sabatier University and the LCC-CNRS for providing us their facilities.

Supplementary Materials: The supporting information contains the ^{1}H, ^{13}C and ^{31}P NMR spectra of the dendritic compounds, as well as ^{31}P MAS NMR, Raman, IR spectra and EDX analyses of the materials. They can be downloaded at:

References

1. K.S. Novoselov, V.I. Fal'ko, L. Colombo, P.R. Gellert, M.G. Schwab, K. Kim, A Roadmap for Graphene. Nature 490 (2012) 192–200.
2. J. Chen, B. Yao, C. Li, G. Shi, An Improved Hummers Method for Eco-Friendly Synthesis of Graphene Oxide. Carbon 64 (2013) 225–229.
3. S. Kochmann, T. Hirsch, O.S. Wolfbeis, Graphenes in Chemical Sensors and Biosensors. TrAC, Trends Anal. Chem. 39 (2012) 87–113.
4. D.R. Dreyer, H.-P. Jia, C.W. Bielawski, Graphene Oxide: A Convenient Carbocatalyst for Facilitating Oxidation and Hydration Reactions. Angew. Chem. Int. Ed. 49 (2010) 6813–6816.
5. X. Sun, Z. Liu, K. Welsher, J.T. Robinson, Goodwin, A.; Zaric, S.; Dai, H. Nano-Graphene Oxide for Cellular Imaging and Drug Delivery. Nano Res 1 (2008) 203–212.
6. X. Yan, B. Li, X. Cui, Q. Wei, K. Tajima, L. Li, Independent Tuning of the Band Gap and Redox Potential of Graphene Quantum Dots. J. Phys. Chem. Lett. *2* (2011) 1119–1124.

7. Z. Liu, J.T. Robinson, X. Sun, H. Dai, PEGylated Nanographene Oxide for Delivery of Water-Insoluble Cancer Drugs. J. Am. Chem. Soc. 130 (2008) 10876–10877.
8. H. Kim, R. Namgung, K. Singha, I.-K. Oh, W.J. Kim, Graphene Oxide-Polyethylenimine Nanoconstruct as a Gene Delivery Vector and Bioimaging Tool. Bioconjug. Chem. 22 (2011) 2558–2567.
9. R.R. Nair, P. Blake, A.N. Grigorenko, K.S. Novoselov, T.J. Booth, T. Stauber, N.M.R. Peres, A.K. Geim, Fine Structure Constant Defines Visual Transparency of Graphene. Science 320 (2008) 1308–1308.
10. A. Gholami, S.A. Hashemi, K. Yousefi, S.M. Mousavi, W.-H. Chiang, S. Ramakrishna, S. Mazraedoost, A. Alizadeh, N. Omidifar, G. Behbudi, 3D Nanostructures for Tissue Engineering, Cancer Therapy, and Gene Delivery. J. Nanomater. 2020 (2020) e1852946.
11. J.I. Paredes, S. Villar-Rodil, A. Martínez-Alonso, J.M.D. Tascón, Graphene Oxide Dispersions in Organic Solvents. Langmuir 24 (2008) 10560–10564.
12. W. Xiao, B. Yan, H. Zeng, Q. Liu, Dendrimer Functionalized Graphene Oxide for Selenium Removal. Carbon 105 (2016) 655-664.
13. D.A. Tomalia, Dendrons/Dendrimers: Quantized, Nano-Element like Building Blocks for Soft-Soft and Soft-Hard Nano-Compound Synthesis. Soft Mater. 6 (2010) 456–474.
14. A. Zibarov, A. Oukhrib, J. Aujard Catot, C.-O. Turrin, A.-M. Caminade, AB5 Derivatives of Cyclotriphosphazene for the Synthesis of Dendrons and Their Applications. Molecules 26 (2021) 4017.
15. J.-P. Majoral, A.-M. Caminade, What to Do with Phosphorus in Dendrimer Chemistry. In New Aspects in Phosphorus Chemistry II; Majoral, J.-P., Ed.; Topics in Current Chemistry; Springer Berlin Heidelberg: Berlin, Heidelberg, 223 (2003) 111–159. ISBN 978-3-540-44086-4.
16. O. Alami, R. Laurent, J.-P. Majoral, N. El Brahmi, S. El Kazzouli, A.-M. Caminade, Copper Complexes of Phosphorus Dendrimers and Their Properties. Inorg. Chim. Acta 517 (2021) 120212.
17. J. Qiu, A. Hameau, X. Shi, S. Mignani, , J.-P. Majoral, A.-M Caminade, Fluorescent Phosphorus Dendrimers: Towards Material and Biological Applications. ChemPlusChem 84 (2019) 1070–1080.
18. J.-P. Majoral, J.M. François, R. Fabre, A. Senescau, S. Mignani, A.-M. Caminade, Multiplexing Technology for in Vitro Diagnosis of Pathogens: The Key Contribution of Phosphorus Dendrimers. Sci. China Mater. 61 (2018) 1454–1461.
19. A.-M. Caminade, Phosphorus Dendrimers for Nanomedicine. Chem. Commun. 53 (2017) 9830–9838.
20. S. Mignani, N. El Brahmi, L. Eloy, J. Poupon, V. Nicolas, A. Steinmetz, S. El Kazzouli, M.M. Bousmina, M. Blanchard-Desce, A.-M. Caminade, Anticancer Copper(II) Phosphorus Dendrimers Are Potent Proapoptotic Bax Activators. Eur. J. Med. Chem. 132 (2017) 142–156.
21. S.M. Mignani, N. El Brahmi, S. El Kazzouli, R. Laurent, S. Ladeira, A.-M. Caminade, E. Pedziwiatr-Werbicka, E.M. Szewczyk, M. Bryszewska, M.M. Bousmina, Original Multivalent Gold(III) and Dual Gold(III)–Copper(II) Conjugated Phosphorus Dendrimers as Potent Antitumoral and Antimicrobial Agents. Mol. Pharmaceutics 14 (2017) 4087–4097.
22. N. El Brahmi, S.M. Mignani, J. Caron, S.E. Kazzouli, M.M. Bousmina, A.-M. Caminade, T. Cresteil, J.-P. Majoral, Investigations on Dendrimer Space Reveal Solid and Liquid Tumor Growth-Inhibition by Original Phosphorus-Based Dendrimers and the Corresponding Monomers and Dendrons with Ethacrynic Acid Motifs. Nanoscale 7 (2015) 3915–3922.
23. N. Launay, A.-M. Caminade, J.-P. Majoral, Synthesis of Bowl-Shaped Dendrimers from Generation 1 to Generation 8. J. Organomet. Chem. 529 (1997) 51–58.
24. O. Rolland, C.-O. Turrin, G. Bacquet, R. Poupot, M. Poupot, A.-M. Caminade, J.-P. Majoral, Efficient Synthesis of Phosphorus-Containing Dendrimers Capped with Isosteric Functions of Amino-Bismethylene Phosphonic Acids. Tetrahedron Lett. 50 (2009) 2078–2082.
25. D. Riegert, A. Pla-Quintana, S. Fuchs, R. Laurent, C.-O. Turrin, C. Duhayon, J.-P. Majoral, A. Chaumonnot, A.-M. Caminade, Diversified Strategies for the Synthesis of Bifunctional Dendrimeric Structures. Eur. J. Org. Chem. 2013 (2013) 5414–5422.
26. E.R. Jong, N. Deloch, W. Knoll, C.-O. Turrin, J.-P. Majoral, A.-M. Caminade, I. Köper, Synthesis and Characterization of Bifunctional Dendrimers: Preliminary Use for the Coating of Gold Surfaces and the Proliferation of Human Osteoblasts (HOB). New J. Chem. 39 (2015) 7194–7205.
27. Q. Vanbellingen, P. Servin, A. Coinaud, S. Mallet-Ladeira, R. Laurent, A.-M. Caminade, Dendrimers Functionalized with Palladium Complexes of N-, N,N-, and N,N,N-Ligands. Molecules 26 (2021) 2333.
28. N. El Brahmi, S. El Kazzouli, S.M. Mignani, E.M. Essassi, G. Aubert, R. Laurent, A.-M. Caminade, M.M. Bousmina, T. Cresteil, J.-P. Majoral, Original Multivalent Copper(II)-Conjugated Phosphorus Dendrimers and Corresponding Mononuclear Copper(II) Complexes with Antitumoral Activities. Mol. Pharmaceutics 10 (2013) 1459–1464.
29. W.S. Hummers, R.E. Offeman, Preparation of Graphitic Oxide. J. Am. Chem. Soc. 80 (1958) 1339–1339.

30. A. Onaș, I. Biru, G. Sorina, H. Iovu, Novel Bovine Serum Albumin Protein Backbone Reassembly Study: Strongly Twisted β-Sheet Structure Promotion upon Interaction with GO-PAMAM. Polymers 12 (2020).
31. A.-M. Caminade, S. Fruchon, C.-O. Turrin, M. Poupot, A. Ouali, A. Maraval, M. Garzoni, M. Maly, V. Furer, V. Kovalenko, J.-P. Majoral, G.M. Pavan, R. Poupot, The key role of the scaffold on the efficiency of dendrimer nanodrugs, Nat. Commun. 6 (2015) 7722.
32. A. Hameau, S. Fuchs, R. Laurent, J.-P. Majoral, A.-M. Caminade, Synthesis of Dye/Fluorescent Functionalized Dendrons Based on Cyclotriphosphazene. Beilstein J. Org. Chem. 7 (2011) 1577–1583.
33. G. Franc, S. Mazères, C.-O. Turrin, L. Vendier, C. Duhayon, A.-M. Caminade, J.-P. Majoral, Synthesis and Properties of Dendrimers Possessing the Same Fluorophore(s) Located Either Peripherally or Off-Center. J. Org. Chem. 72 (2007) 8707–8715.